Dynamic Configuration on a Chiral-at-rhodium Catalyst Featuring a Flexible Tetradentate Ligand

Alvaro G. Tejero, Javier Castillo, Fernando Viguri*, Daniel Carmona, Vincenzo Passarelli, Fernando J. Lahoz, Pilar García-Orduña and Ricardo Rodríguez*

[a] Alvaro G. Tejero, Javier Castillo, Dr. Fernando Viguri, Dr. Daniel Carmona, Dr. Vincenzo Passarelli, Dr. Fernando J. Lahoz, Dr. Pilar García-Orduña and Dr. Ricardo Rodríguez
Departamento de Catálisis y Procesos Catalíticos, Departamento de Química Inorgánica
Instituto de Síntesis Química y Catálisis Homogénea (ISQCH), CSIC - Universidad de Zaragoza
Pedro Cerbuna 12, 50009 Zaragoza, Spain
E-mail: riromar@unizar.es; fviguri@unizar.es

Supporting information for this article is given via a link at the end of the document.

Abstract: The unique dynamic configuration of an enantioselective chiral-at-metal catalyst based on Rh(III) and a non-chiral tetradentate ligand is described and resolved. At room temperature, the catalyst undergoes a dynamic configuration process leading to the formation of two interconvertible metal-stereoisomers, remarkably without racemization. Density functional theory (DFT) calculations indicate that this metal-isomerization proceeds *via* a concerted transition state, which features a trigonal bipyramidal geometry stabilized by the tetradentate ligand. Furthermore, the resolved enantiopure complex shows high catalytic enantioinduction in the Friedel-Crafts reaction, achieving enantiomeric ratios as high as 99:1.

The efficiency of chiral metal catalysts hinges on design. Traditionally, chiral transition metal catalysts have relied on chiral ligands,[1] but a more recent approach positions the metal itself as the primary source of chirality.[2] In this strategy, the metal cation is surrounded by achiral ligands and is the exclusive stereogenic element. Due to the structural simplicity coupled with the smart design of the chiral pocket, chiral-at-metal catalysts hold enormous potential in order to expand the scope of chiral catalysis and its implementation in asymmetric synthesis.[2]

The main challenge in chiral-at-metal catalysts lies in achieving high configurational stability at the stereogenic metal center, even in the presence of labile ancillary ligands that are essential for the eventual interaction of the substrate with the metal center and its activation. Only a few stable catalysts with labile ancillary ligands are known (Scheme 1). Most are based on octahedral complexes with d^6 transition metals and two inert bidentate ligands that exert the stereogenic control at the metal center, effectively precluding racemization processes. Intriguingly, the development of chiral-at-metal catalysts with metal-isomerization-mediated dynamic configuration[3] remains an unexplored avenue.

Early studies on stable chiral-at-metal catalysts typically employed metal complexes bearing two neutral bidentate ligands (**I**).[4] Unfortunately, these catalysts generated limited enantioselectivity. Nevertheless, in 2014, Meggers and coworkers developed well-defined chiral-at-metal catalysts (**II**) with two monoanionic chelate ligands,[5] proving that enantioselectivities exceeding 95:5 could be attained in a wide range of reactions, including Lewis acid[6] and redox[7] catalysis. Grubbs and Hartung

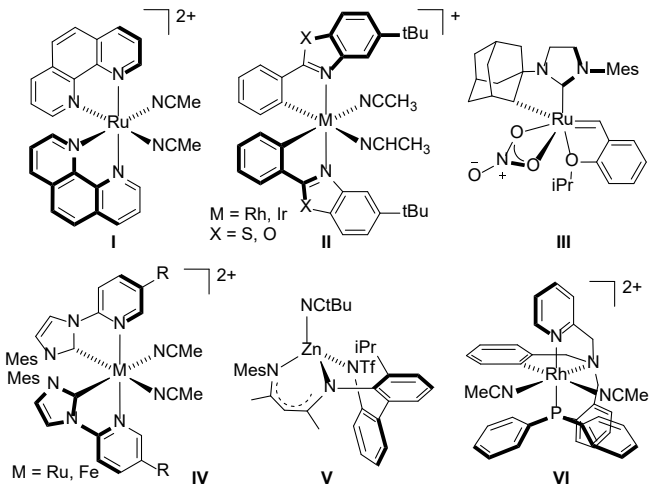

Scheme 1. Stable chiral-at-metal catalysts.

discovered that a monoanionic chelate carbene ligand could stabilize the configuration at a ruthenium center (**III**).[8] Subsequently, Meggers *et al.* designed a new class of chiral-at-metal octahedral catalysts based on Ru(II) and Fe(II) (**IV**) with two neutral non-symmetric pyridine-carbene ligands that efficiently transfer chirality.[9] To the best of our knowledge, only two types of chiral-at-metal catalysts with polydentate ligands have been reported. In 2020, Sihonoya and coworkers introduced the Zn(II) complex **V** bearing a tridentate monoanionic ligand with a robust configuration that exhibited high enantioinduction in Diels-Alder reaction.[10] In 2018, our group developed the Rh(III) solvate **VI** with a tripodal tetradentate ligand.[11] In this case, the inert κ^4C,N,N',P coordination of the ligand ensures the configuration stability at the metal, enabling it to efficiently induce chirality.

Herein, we report on the chiral-at-rhodium solvate complex $[Rh(\kappa^4C,N,O,P\text{-}\mathbf{L_O})(NCMe)_2][SbF_6]$ (**5**) (Scheme 2), which exhibits a dynamic configuration compatible with the stereogenic metal information. After resolving **5**, its activity as a catalyst of the Friedel-Craft reaction has been assessed, observing enantiomeric ratios up to 99/1.

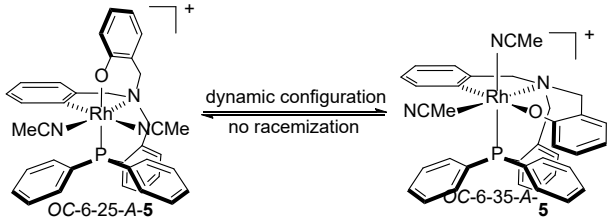

Scheme 2. This work.

The reaction of the trichorido rhodium complex [$RhCl_3$(κ³*N*,*O*,*P*-**HL$_{OH}$**)] (**1**) with 1 equiv of NEt_3 in acetonitrile at 60 °C resulted in the formation of the tetracoordinate rhodium complex [$RhCl_2$(κ⁴*C*,*N*,*O*,*P*-**L$_{OH}$**)] (**2**) in good yield (Scheme 3). In the NMR spectra of **2** only one set of signals is observed. Indeed, the $^{31}P\{^1H\}$ NMR spectrum displays a doublet at 34.21 ppm ($^1J_{Rh-P}$ = 141.2 Hz). In ^1H NMR spectrum, the OH group coordinated to the rhodium appears at 16.18 ppm, at 5.6 ppm lower field than in the free ligand.

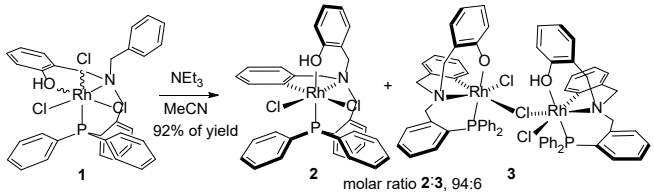

Scheme 3. Synthesis of the chlorido complexes **2** and **3**.

The IR spectrum of **2** contains a broad band at 3474 cm^{-1} assigned to the OH stretching.[12] The three methylene groups resonate (^1H) as diastereotopic protons: $(CH_2)O$ at 6.92 and 3.22 ppm, $(CH_2)P$ at 6.92 and 3.74 ppm, and $(CH_2)C$ at 4.03 and 3.34 ppm. The $^{13}C\{^1H\}$ NMR signal at 156.64 ppm (dd) with $^1J_{Rh-C}$ = 30.1 and $^2J_{P-C}$ = 10.3 Hz confirms the C−Rh bond in complex **2**. The observed nuclear Overhauser effect (NOE) pattern indicates a P−Rh−O *trans* disposition for **2**.

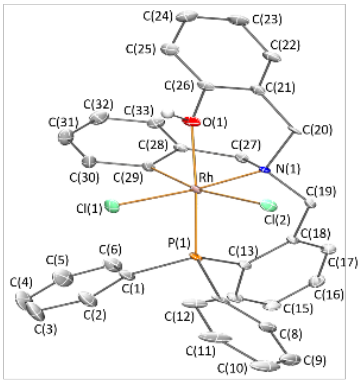

Figure 1. X-ray structure of **2**. Except for OH, H atoms are omitted for clarity.

The crystal structure of **2**[13] reveals the stereogenic rhodium in an octahedral geometry, with our coordinating atoms of **L$_{OH}$** and the chlorido ligands occupying two *cis* coordination sites (Figure 1). The coordinated phosphorus atom is *trans* to the oxygen atom O(1), while the chlorine atoms Cl(1) and Cl(2) are *trans* to N(1) and C(29), respectively. The Rh−Cl(2) bond length (2.4923(12) Å) is larger than Rh−Cl(1) (2.3587(11) Å) reasonably due to the different *trans* influence of N(1) vs. C(29). The rhodium-oxygen bond in **2** [Rh−O(1), 2.191(3) Å] is a little longer than in [$RhCl_2$(salcen)] (Rh−O, 2.143(3) Å; salcen = *trans*-1,2-diaminocyclohexane-*N*,*N*′-bis(3,5-di-tert-butylsalicylidene),[14] suggesting a dative ligation mode.

Complex **2** precipitates from the reaction medium together with a minor amount of **3** (about 6%) (Scheme 3 and SI). NMR analysis of the mixture of **2** and **3** in the presence of HCl suggests the establishment of the equilibrium reaction 2 × **2** ⇄ **3** + HCl (SI). Remarkably, complex **2** exhibits exceptional stability, even in the presence of an excess of HCl, highlighting the robustness of the Rh−C bond.[15]

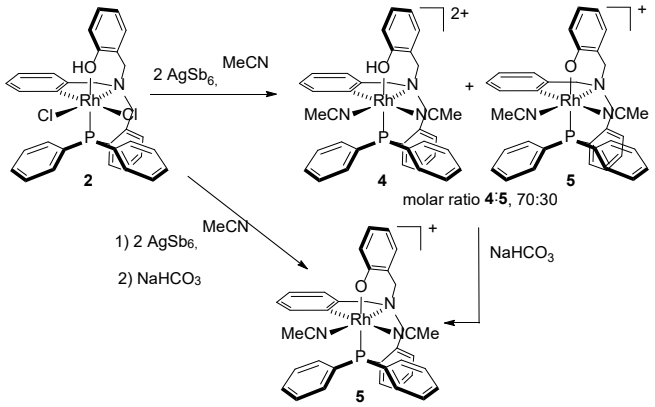

Scheme 4. Synthesis of the solvato complexes.

To enable two accessible coordination sites in the chiral-at-rhodium catalyst, the dichlorido complex **2** was treated with $AgSbF_6$ in acetonitrile (Scheme 4). The reaction yields a mixture of [Rh(κ⁴*C*,*N*,*O*,*P*-**L$_{OH}$**)$(NCMe)_2$][SbF_6]$_2$ (**4**) and [Rh(κ⁴*C*,*N*,*O*,*P*-**L$_O$**)$(NCMe)_2$][SbF_6] (**5**) (molar ratio **4**:**5**, 65:35), with the protonated and deprotonated RhOH fragment, respectively. When $NaHCO_3$ was added to the initial reaction mixture or to the mixture of **4** and **5**, only complex **5** was obtained (see SI). Upon crystallization of **4** in THF/Et_2O, single crystals of **4'** were obtained, instead (Figure 2). Complex **4'** shows an octahedral geometry of the metal center, with the rhodium atom coordinated by the ligand (κ⁴*C*,*N*,*O*,*P*)-**L$_{OH}$**, an acetonitrile group, and a water molecule that

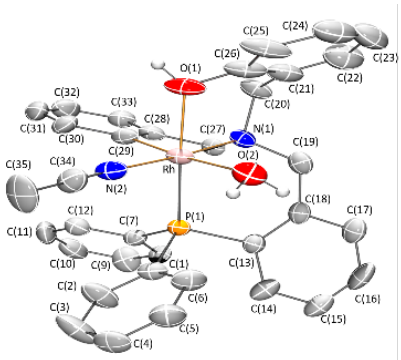

Figure 2. X-ray structure of solvate **4'**. Except for OH and coordinated water, H atoms are omitted for clarity.

replaces the initial MeCN molecule in **4**. The O(1) atom, *trans* to P(1), has a bond length to Rh(1) (2.146(4) Å) between Rh−O(phenoxo) bond lengths in **2** (2.191(3) Å) and **3** (2.1258(13) Å). Henceforth, our investigations primarily centered on **5**, which was isolated with a 94% yield.

In CD_2Cl_2 at room temperature, the $^{31}P\{^1H\}$ spectrum of **5** shows a broad signal at 33.0 ppm. At -30 °C, a single sharp doublet centered at 34.01 ppm (d, $^1J_{Rh\text{-}P}$ = 121.7 Hz) is observed. At the same temperature, the proton spectrum presents a unique set of well-defined signals. NOESY experiments confirm that *trans* disposition of the oxygen and phosphorus atoms of the doubly deprotonated ligand (κ^4*C*,*N*,*O*,*P*)-**L**$_\mathbf{O}$. Intriguingly, EXSY (^{1}H-^{1}H) experiments indicate that the MeCN ligand *trans* to the carbon (s, 1.84 ppm) exchanges with free acetonitrile (s, 2.05 ppm), suggesting that complex **5** might serve as a catalytic precursor.

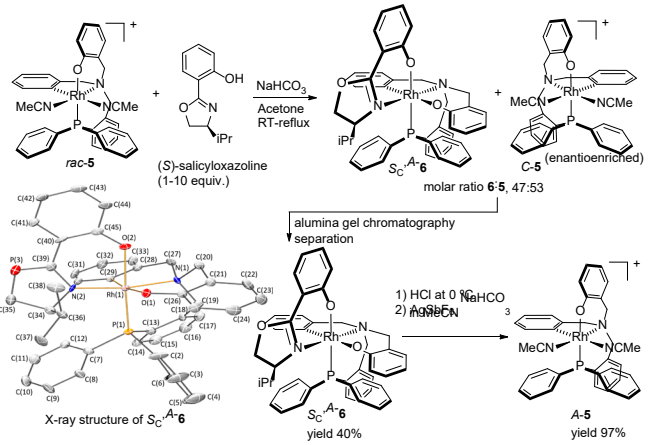

Scheme 5. (*S*)-Salicyloxazoline mediated resolution of complex 5 and X-ray structure of diastereomer *S*$_C$,*A*-6.

The racemic complex **5** (*rac*-**5**) has been resolved using the chiral auxiliary (*S*)-2-(4-isopropyl-4,5-dihydrooxazol-2-yl)phenol ((*S*)-salicyloxazoline), following the methodology outlined in Scheme 5. At room temperature, treatment of *rac*-**5** with 10 equivalents of (*S*)-salicyloxazoline in the presence of $NaHCO_3$ (4 equiv) in acetone leads to the formation of only one new metal complex, namely **6** (Scheme 5, top). Compound **6** exhibits a sharp ^{31}P NMR doublet at 21.14 ppm ($J_{Rh\text{-}P}$ = 140.6 Hz). In addition, unreacted complex **5** is detected, accounting for 53% of the total initial sample. After 48 hours of refluxing in acetone, the composition of the mixture remains constant still presenting the molar ratio **5**:**6**, 53:47. The constant ratio of **5** and **6** in the presence of a large excess of (*S*)-salicyloxazoline (10 equiv) (Scheme 5, top) demonstrates the exclusive formation of **6** and suggests that solvate complex **5** does not undergo racemization at the stereogenic metal center. Hence, the unreacted compound **5** is expected to be enantioenriched.

In agreement with the experimental data, DFT calculations at the B97D3/def2svp level reveal that **6** is 4-8 kcal·mol^{-1} more stable than other potential isomers (**I**-**VII**, Figure SI-7). A thorough examination of the calculated structures of **6** and its isomers revealed that the reduced steric congestion at the metal center in **6** might cause its higher stability with respect to its isomers.

After alumina gel chromatography separation, compound **6** was isolated as a diastereomerically pure crystalline solid with a 40% yield (Scheme 5, bottom; see SI).[16] NMR and X-ray diffraction studies confirm the presence of a stereogenic rhodium center (see Scheme 5, bottom; see SI). In the resulting diastereomer *S*$_C$-*OC*-6-26-**6**, the absolute configuration at the metal center is anticlockwise (*A*).[17] Noticeably, in diastereomer *S*$_C$-*OC*-6-26-*A*-**6** (*S*$_C$,*A*-**6**), the carbon atom of the ligand (κ^4*C*,*N*,*O*,*P*)-**L**$_\mathbf{O}$ lies *trans* to the O(phenoxo) group. This arrangement differs from that found in all previous complexes (**2**-**5**) and involves the metal-isomerization process by means of the formal migration of the O(phenoxo) group. Given the labile nature of one of the NCMe ligands and the nucleophilic oxygen atom in **5**, we propose that the migration process occurs within the solvate complex **5** before its interaction with the chiral auxiliary, as depicted in Scheme 6.

Upon addition of HCl (7 equiv) at 0 °C, diastereomer *S*$_C$,*A*-**6**, yields the enantioenriched dichlorido complex *OC*-6-25-*A*-**2** (*A*-**2**) in 94% of yield (Scheme 5, bottom). The subsequent treatment of *A*-**2** with $AgSbF_6$ and $NaHCO_3$ in CH_3CN results in the formation of the optically active solvate complex *OC*-6-25-*A*-**5** (*A*-**5**) (Scheme 5, bottom). Notably, the phenoxo group of the ligand (κ^4*C*,*N*,*O*,*P*)-**L**$_\mathbf{O}$ migrates once again, lying *trans* to the phosphorus atom in complexes *A*-**2** and *A*-**5**.

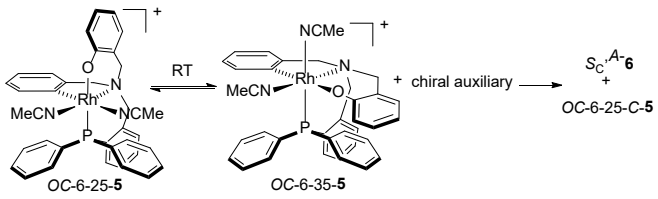

Scheme 6. Metal-isomerization process.

It is important to emphasize that the retention of chirality in chiral-at-metal complexes is not initially apparent due to the flexibility of the coordination geometry, which is enhanced by the lability of the ligand-metal bonds. The racemization process is a huge concern when dealing with chiral-at-metal catalytic systems, and several associative and dissociative mechanisms have been proposed to explain racemization at stereogenic metal complexes.[18] In our case, despite two labile positions and a migrating phenoxo arm, chiral-at-rhodium complex *A*-**5** preserves its chiral information at the stereogenic metal. Circular dichroism studies of enantioenriched *A*-**5** indicate that, in THF, the racemization of the stereogenic metal is not observed, or at least it is not significant over 24 hours (SI).

Considering the striking dynamic configuration at rhodium in *A*-**5**, we performed DFT calculations at the B97D3/def2svp level to gain insight into the metal-isomerization process (Figure 3). In agreement with the observed formation of *OC*-6-25-**5**, the isomer *OC*-6-35-**5** was calculated to be 3.1 kcal·mol^{-1} less stable than *OC*-6-25-**5**. Nonetheless, the formation of *OC*-6-35-**5** (as the step previous to the reaction with (*S*)-salicyloxazoline affording **6**) is accessible and reversible. Indeed *OC*-6-25-**5** should undergo the dissociation of the CH_3CN ligand *trans* to the carbon atom rendering the square pyramidal intermediate **VIII** (+4.9 kcal·mol^{-1}), which in turn isomerizes to the square pyramidal complex **IX** (+7.4 kcal·mol^{-1}) *via* the transition state **TS_VIII-IX** (+13.3 kcal·mol^{-1}) as a result of the non-dissociative migration of the phenoxo arm (Figure 3). Finally, the coordination of one CH_3CN molecule to **IX** renders *OC*-6-35-**5**. Likely, the concerted migration process guarantees that no racemization at the stereogenic rhodium center may take place.

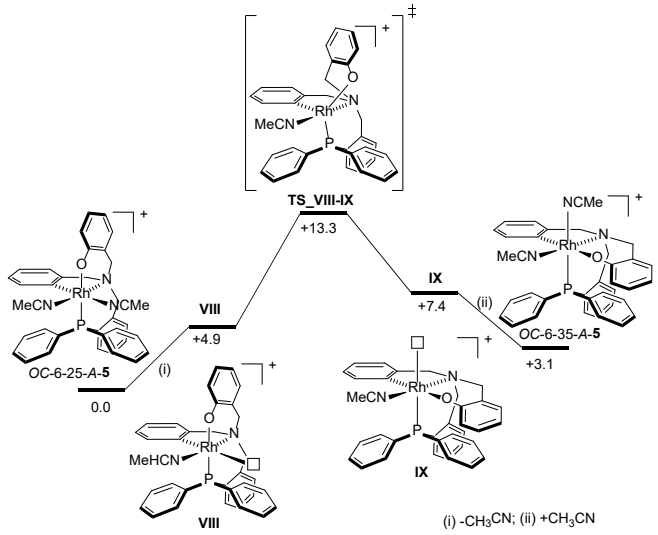

Figure 3. Gibbs free energy profile for the reaction *OC*-6-25-**5** ⇆ *OC*-6-35-**5** (kcal·mol^{-1}, B97D3/def2svp, 298 K, 1 atm, CPCM/CH_2Cl_2).

We performed a proof-of-concept study to assess the capacity of the chiral-at-metal complex *A*-**5** to transfer chiral information in the course of a catalytic process. Specifically, *A*-**5** was tested as a catalyst in the Friedel-Crafts reaction between NH-indole and (2*E*)-1-(1-methyl-1*H*-imidazol-2-yl)-2-buten-1-one. The reaction requires several hours to achieve satisfactory conversions, with enantiomeric ratios of up to 99/1. Interestingly, even when *A*-**5** was stored in solution for 24 and 72 hours before catalysis (Table 1, entries 3-5), the efficiency of *A*-**5** to induce chirality was observed to be the same. This finding strongly indicates that the metal-isomerization process does not involve racemization of the stereogenic rhodium center and, therefore, does not impact the enantioselectivity of the catalytic outcome.

Table 1. Friedel-Crafts alkylation catalyzed by *A*-**5a**.

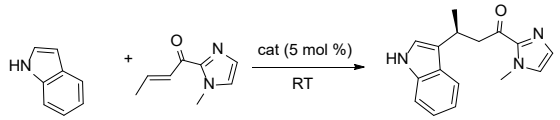

Entry	Cat	Solv	Storage time (h)	t (h)	Conv (%)[b]	e.r.[c]
1	rac-**5**	EtOAc	-	70	67	-
2	rac-**5**	THF	-	22	93	-
3	rac-**2**	THF	-	188	-	-
4	*A*-**5**	THF	0	22	90	99/1
6	*A*-**5**	THF	24	22	92	98/2
7	*A*-**5**	THF	72	22	91	99/1

[a]Reaction conditions: catalyst 0.736 mM (5.0 mol %), 2-buten-1-one 18.40 mM, and indole 14.72 mM in 3 mL of solvent. [b]Based on indole. Determined by ^{1}H NMR. [c]Determined by chiral HPLC.

In conclusion, we have successfully synthesized and resolved the original chiral-at-metal *A*-**5**, which exhibits a dynamic configuration at rhodium center. Notably, this dynamic configuration process takes place at room temperature without a lack of chiral information. The transformation is mediated through a concerted transition state involving the coordinated (κ^4*C*,*N*,*O*,*P*)-$\mathbf{L_O}$ ligand. The high degree of enantioinduction observed, up to 99/1, highlights the potential utility of chiral-at-metal catalysts based on ligands with labile metal-ligand bonds in asymmetric catalysis.

Supporting Information

The authors have cited additional references within the Supporting Information.[19-29]

Acknowledgements

We thank the Ministerio de Ciencia, Innovación y Universida-des (MCIU) of Spain, Agencia Estatal de Investigación (AEI) of Spain, Fondo Europeo de Desarrollo Regional (FEDER) (CTQ2018-095561-BI00 and PID2021-122406NB-I00) and Gobierno de Aragón (Grupo de Referencia: Catálisis Homogé-nea Enantioselectiva E05_23R) for financial support. V. P. thanks the resources from the supercomputer “Memento”, and the technical expertise and assistance provided by the Institute for Biocomputation and Physics of Complex Systems (BIFI) Universidad de Zaragoza. F. J. L and P. G-O. acknowledge the Thematic network “CrysFact”, ref. RED2018-102574-T (MCIU/AEI) for its support. X-ray dif-fraction experiments were performed at XALOC beamline at ALBA Synchrotron with the collaboration of ALBA staff.

Keywords: asymmetric catalysis • catalyst design • chiral-at-metal • dynamic configuration • rhodium

[1] P. J. Walsh, M. C. Kozlowski, *Fundamentals of Asymmetric Catalysis*; University Science Books: Sausalito, Calif, **2009**.

[2] a) P. S. Steinlandt, L. Zhang, E. Meggers, *Chem. Rev.* **2023**, *123*, 4764–4794. b) R. Rodríguez, V. Passarelli, D. Carmona, Carbon–Carbon Bond Formation Via Stereogenic-Only-at-Metal Chiral Catalysts. In *Reference Module in Chemistry, Molecular Sciences and Chemical Engineering*; Elsevier, **2022**; p B9780323906449000000. c) L. Zhang, E. Meggers, *Chem. Asian J.* **2017**, *12*, 2335–2342. d) L. Zhang, E. Meggers, *Acc. Chem. Res.* **2017**, *50*, 320–330.

[3] a) S. Akine, H. Miyake, *Coordination Chemistry Reviews* **2022**, *468*, 214582. b) E. Meggers, *Chem. Eur. J.* **2010**, *16*, 752–758.

[4] a) M. Chavarot, S. Ménage, O. Hamelin, F. Charnay, J. Pécaut, M. Fontecave, *Inorg. Chem.* **2003**, *42*, 4810–4816. b) C. Ganzmann, J. A. Gladysz, *Chem. Eur. J.* **2008**, *14*, 5397–5400.

[5] a) H. Huo, C. Fu, K. Harms, E. Meggers, *J. Am. Chem. Soc.* **2014**, *136*, 2990–2993. b) C. Wang, L.-A. Chen, H. Huo, X. Shen, K. Harms, L. Gong, E. Meggers, *Chem. Sci.* **2015**, *6*, 1094–1100.

[6] a) C. Wang, L.-A. Chen, H. Huo, X. Shen, K. Harms, L. Gong, E. Meggers, *Chem. Sci.* **2015**, *6*, 1094–1100. b) L. Feng, X. Dai, E. Meggers, L. Gong, *Chem. Asian J.* **2017**, *12*, 963–967. c) C. Ye, S. Chen, F. Han, X. Xie, S. Ivlev, K. N. Houk, E. Meggers, *Angew. Chem. Int. Ed.* **2020**, *59*, 13552–13556. d) L. Hu, S. Lin, S. Li, Q. Kang, Y. Du, *ChemCatChem* **2020**, *12*, 118–121.

[7] a) H. Huo, X. Shen, C. Wang, L. Zhang, P. Röse, L.-A. Chen, K. Harms, M. Marsch, G. Hilt, E. Meggers, *Nature* **2014**, *515*, 100–103. b) H. Huo, K. Harms, E. Meggers, *J. Am. Chem. Soc.* **2016**, *138*, 6936–6939. c) J. Ma, X. Zhang, X. Huang, S. Luo, E. Meggers, *Nat Protoc* **2018**, *13*, 605–632. d) X. Huang, Q. Zhang, J. Lin, K. Harms, E. Meggers, *Nat Catal* **2018**, *2*, 34–40.

[8] a) J. Hartung, R. H. Grubbs, *J. Am. Chem. Soc.* **2013**, *135*, 10183–10185. b) J. Hartung, P. K. Dornan, R. H. Grubbs, *J. Am. Chem. Soc.* **2014**, *136*, 13029–13037.

[9] a) Y. Zheng, Y. Tan, K. Harms, M. Marsch, R. Riedel, L. Zhang, E. Meggers, *J. Am. Chem. Soc.* **2017**, *139*, 4322–4325. b) Y. Hong, L. Jarrige, K. Harms, E. Meggers, *J. Am. Chem. Soc.* **2019**, *141*, 4569–4572. c) G. Wang, Z. Zhou, X. Shen, S. Ivlev, E. Meggers, *Chem. Commun.* **2020**, *56*, 7714–7717.

[10] a) K. Endo, Y. Liu, H. Ube, K. Nagata, M. Shionoya, *Nat Commun* **2020**, *11*, 6263. b) Y. Liu, H. Ube, K. Endo, M. Shionoya, *ACS Org. Inorg. Au* **2023**, acsorginorgau.3c00026.

[11] a) M. Carmona, R. Rodríguez, V. Passarelli, F. J. Lahoz, P. García-Orduña, D. Carmona, *J. Am. Chem. Soc.* **2018**, *140*, 912–915. b) M. Carmona, R. Rodríguez, V. Passarelli, D. Carmona, *Organometallics* **2019**, *38*, 988–995. c) A. G. Tejero, M. Carmona, R. Rodríguez, F. Viguri, F. J. Lahoz, P. García-Orduña, D. Carmona, *RSC Adv.* **2022**, *12*, 34704–34714.

[12] L. Biancalana, G. Ciancaleoni, S. Zacchini, A. Monti, F. Marchetti, G. Pampaloni, *Organometallics* **2018**, *37*, 1381–1391.

[13] Deposition numbers 2295813 (for **2**), 2295814 (for **3**), 2295815 (for **4'**) and 2295816 (for **6**) contain the supplementary crystallographic data for this paper. These data are provided free of charge by the joint Cambridge Crystallographic Data Centre and Fachinformationszentrum Karlsruhe Access Structures service.

[14] a) R. A. Stinziano-Eveland, S. T. Nguyen, L. M. Liable-Sands, A. L. Rheingold, *Inorg. Chem.* **2000**, *39*, 2452–2455. b) H. Inoue, J. Ito, M. Kikuchi, H. Nishiyama, *Chem. Asian J.* **2008**, *3*, 1284–1288. c) R. Siefert, T. Weyhermüller, P. Chaudhuri, *J. Chem. Soc., Dalton Trans.* **2000**, 4656–4663.

[15] No dissociation of the OH group was observed by ^{1}H and ^{31}P NMR spectroscopy, despite the potential hemilability of the phenolic arm in **2**.

[16] Limited amounts of enantioenriched in *C*-**5** were also obtained, although the enantiomer ratio can not be quantified.

[17] N. G. Connelly, T. Damhus, R. H. Hartshorn, A. T. Hutton, Nomenclature of Inorganic Chemistry, IUPAC Recommendations **2005**, RSC Publishing, Cambridge, UK. Chapter IR-9.3.4.8, p. 189.

[18] a) Q. Gaydon, D. S. Bohle, *Inorg. Chem.* **2021**, *60*, 13567–13577. b) Q. Gaydon, D. S. Bohle, *Inorg. Chem.* **2022**, *61*, 4660–4672. c) D. C. Ashley, E. Jakubikova, *Inorg. Chem.* **2018**, *57*, 5585–5596. d) G. Dhimba, A. Muller, K. Lammertsma, *Inorg. Chem.* **2022**, *61*, 14918–14923. e) L. Gong, M. Wenzel, E. Meggers, *Acc. Chem. Res.* **2013**, *46*, 2635–2644. f) M. Carmona, R. Rodríguez, I. Méndez, V. Passarelli, F. J. Lahoz, P. García-Orduña, D. Carmona, *Dalton Trans.* **2017**, *46*, 7332–7350. g) W. J. Maximuck, C. Ganzmann, S. Alvi, K. R. Hooda, J. A. Gladysz, *Dalton Trans.* **2020**, *49*, 3680–3691. h) H. Brunner, T. Tsuno, *Acc. Chem. Res.* **2009**, *42*, 1501–1510. i) T. Wititsuwannakul, M. B. Hall, J. A. Gladysz, *Organometallics* **2021**, *40*, 742–759. j) D. Carmona, M. P. Lamata, F. Viguri, R. Rodríguez, F. J. Lahoz, L. A. Oro, *Chem. Eur. J.* **2007**, *13*, 9746–9756. k) D. Carmona, M. P. Lamata, F. Viguri, E. San José, A. Mendoza, F. J. Lahoz, P. García-Orduña, R. Atencio, L. A. Oro, *Journal of Organometallic Chemistry* **2012**, *717*, 152–163.

[19] J. Juanhuix, F. Gil-Ortiz, G. Cuní, C. Colldelram, J. Nicolás, J. Lidón, E. Boter, C. Ruget, S. Ferrer, J. Benach, *J. Synchr. Rad.* **2014**, *21*, 679-689.

[20] SAINT+, version 6.01: Area-Detector Integration Software, Bruker AXS, Madison, WI, 2001.

[21] SADABS, Area Detector Absorption Program. Bruker AXS, Madison, WI, 1996; L. Krause, R. Herbst-Irmer, G. M. Sheldrick, D. Stalke, *J. Appl. Cryst.* **2015**, *48*, 3–10.

[22] G. M. Sheldrick, A short history of SHELX. *Acta Crystallogr.* **2008**, *A64*, 112–122.

[23] G. M. Sheldrick, Crystal structure refinement with SHELXL. *Acta Crystallogr.* **2015**, *C71*, 3–8.

[24] O. V. Dolomanov, L. J. Bourhis, R. J. Gildea, J. A. K. Howard, H. Puschmann, *J. Appl. Crystallogr.* **2009**, *42*, 339-341.

[25] Gaussian 16, Revision C.01, M. J. Frisch, G. W. Trucks, H. B. Schlegel, G. E. Scuseria, M. A. Robb, J. R. Cheeseman, G. Scalmani, V. Barone, G. A. Petersson, H. Nakatsuji, X. Li, M. Caricato, A. V. Marenich, J. Bloino, B. G. Janesko, R. Gomperts, B. Mennucci, H. P. Hratchian, J. V. Ortiz, A. F. Izmaylov, J. L. Sonnenberg, D. Williams-Young, F. Ding, F. Lipparini, F. Egidi, J. Goings, B. Peng, A. Petrone, T. Henderson, D. Ranasinghe, V. G. Zakrzewski, J. Gao, N. Rega, G. Zheng, W. Liang, M. Hada, M. Ehara, K. Toyota, R. Fukuda, J. Hasegawa, M. Ishida, T. Nakajima, Y. Honda, O. Kitao, H. Nakai, T. Vreven, K. Throssell, J. A. Montgomery, Jr., J. E. Peralta, F. Ogliaro, M. J. Bearpark, J. J. Heyd, E. N. Brothers, K. N. Kudin, V. N. Staroverov, T. A. Keith, R. Kobayashi, J. Normand, K. Raghavachari, A. P. Rendell, J. C. Burant, S. S. Iyengar, J. Tomasi, M. Cossi, J. M. Millam, M. Klene, C. Adamo, R. Cammi, J. W. Ochterski, R. L. Martin, K. Morokuma, O. Farkas, J. B. Foresman, and D. J. Fox, Gaussian, Inc., Wallingford CT, **2016**.

[26] A. D. Becke, *J. Chem. Phys.*, **1997**, *107*, 8554-8560.

[27] S. Grimme, S. Ehrlich, L. Goerigk, *J. Comp. Chem.*, **2011**, *32*, 1456–1465.

[28] F. Weigend, R. Ahlrichs, *Phys. Chem. Chem. Phys.*, **2005**, *7*, 3297–3305.

[29] J. Tomasi, B. Mennucci, R. Cammi, *Chem. Rev.*, **2005**, *105*, 2999–3093.

Entry for the Table of Contents

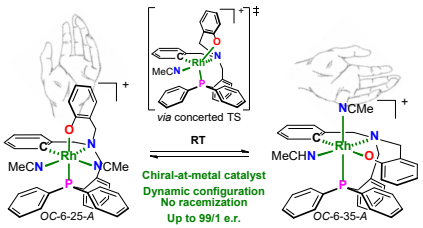

The first chiral-at-metal catalyst with a dynamic configuration has been successfully synthesized and subsequently resolved. Both experimental and DFT studies show that the stereogenic rhodium center preserves its chiral information. Furthermore, the resolved complex provides enantiomeric ratios of up to 99:1 in the catalytic Friedel-Crafts alkylation of indoles. These findings highlight its immense potential in asymmetric catalysis.

Institute and/or researcher Twitter usernames: ((optional))